


Original article

Foam stabilization mechanism of core-shell particles: Insights from the gas-liquid interface theory

Zhengxiao Xu^{1,2}, Guangzhe Ding², Lei Tao², Wenyang Shi², Jiajia Bai², Faqiang Dang^{1,3}

¹State Key Laboratory of Deep Oil and Gas, China University of Petroleum (East China), Qingdao 266580, P. R. China

²School of Petroleum and Natural Gas Engineering, Changzhou University, Changzhou 213164, P. R. China

³School of Mining and Petroleum Engineering, Faculty of Engineering, University of Alberta, Edmonton T6G 1H9, Canada

Keywords:

Deep reservoir
high-temperature and high-salinity
foam performance
core-shell particle
interface effect

Cited as:

Xu, Z., Ding, G., Tao, L. Shi, W., Bai, J., Dang, F. Foam stabilization mechanism of core-shell particles: Insights from the gas-liquid interface theory. *Capillarity*, 2025, 16(1): 5-17.

<https://doi.org/10.46690/capi.2025.07.02>

Abstract:

To improve oil displacement efficiency under deep reservoir conditions, foam flooding technology represents a critical strategy through the establishment of a stable, long-lasting foam system. A central challenge in this application is to characterize the evolution dynamics of foam under extreme reservoir conditions such as high temperature and salinity. In this study, a performance evaluation experiment of foams generated by different types of surfactants was carried out by using the Waring-blender method. The foam stability characteristics were analyzed on the basis of foam volume, half-life of the liquid solution, and the foam comprehensive index and other related parameters. Based on the microscopic action mechanism of gas-liquid interface, the change pattern of foam performance with concentration, salinity and the coordinated action of core-shell particles were investigated. Both candidate surfactants exhibited good resistance to temperature and salinity. Among them, one surfactant demonstrated superior overall performance, with the foam comprehensive index reaching its peak at an optimal mass concentration of 0.5%. In high-salinity environments, the synergistic interaction between core-shell particles and surfactant molecules significantly enhances foam stability. In particular, the combination of this surfactant with core-shell particles at a mass fraction of 0.5% resulted in a notably higher foam comprehensive index, suggesting its strong application potential. This study quantitatively analyzes the synergistic stability effects of salinity, core-shell particles and surfactant, and reveals the synergistic stability mechanism of salt ion compression electric double layer and particle interface adsorption, providing important theoretical guidance for the development and application of deep reservoir foam flooding.

1. Introduction

As a pivotal technology for enhanced oil recovery, foam flooding systems derive their efficacy from maintaining long-term structural stability to control propagation patterns and optimize displacement efficiency. In particular, CO₂ foam systems have emerged as a focal area of research within the global energy transition framework, offering dual func-

tionality by simultaneously enabling enhanced oil recovery along with carbon capture, utilization and storage (Zhou et al., 2024). The Jamin effect-mediated permeability modulation of CO₂ foam systems facilitates the selective plugging of high-permeability zones, thereby expanding sweep efficiency while promoting geological CO₂ sequestration through dissolution and mineral trapping mechanisms—a critical pathway

toward carbon neutrality objectives (Dehdari et al., 2024; Li et al., 2024b). However, the dynamic behavior of foam systems under combined high-temperature/high-pressure conditions, hypersaline environments and heterogeneous porous media remains inadequately characterized, representing significant technical barriers to field implementation.

Fundamental to foam stability enhancement are the mitigation of liquid film drainage kinetics and the suppression of bubble coalescence events. Early investigations employing the Ross-Miles method established the concentration-dependent threshold behavior of surfactant systems, demonstrating foam-ing volume saturation upon exceeding the critical micelle concentration (Vavra et al., 2020). Advanced characterization via cryogenic scanning electron microscopy further elucidated the direct correlation between interfacial film thickness and foam half-life, with surfactant molecular packing density emerging as the primary determinant of interfacial film integrity (Gbadamosi et al., 2025). While polymer-surfactant composite formulations have been developed to exploit the viscoelastic effects of polymers for drainage retardation (Shao et al., 2023; Bersenev et al., 2025), their performance in high-salinity environments remains compromised by salt ion-induced electric double layer compression, which phenomenon promotes surfactant micellization and destabilizes interfacial complexes (Bello et al., 2024).

Due to their unique physicochemical properties, nanoparticles are increasingly employed as foam stabilizers, thereby improving oil displacement efficiency and reservoir performance. As a result, the stabilization of CO₂ foam using nanoparticles has attracted substantial research interest (Sun et al., 2024b). Pickering foams, which are stabilized by solid particles known as Pickering stabilizers, achieve stability through particle adsorption at the gas-liquid interface. Owing to their excellent stability, tunability, functional diversity, and low environmental impact, Pickering foams stabilized with nanomaterials offer promising avenues for advanced foam applications (Sun et al., 2024a). Furthermore, the stimuli-responsive behavior and film-forming capabilities of polymer-based particles provide inspiration for the development of functional, precisely engineered particle-stabilized foams and related materials (Fujii, 2024). The introduction of core-shell particles opens up a new direction for studying the foam stability mechanism (Akamine et al., 2024). Zhang et al. (2023), through an interfacial tension test, found that the particles are adsorbed on the gas-liquid interface by hydrophobic interaction, forming a mechanical barrier to delay drainage. Combined with quartz crystal microbalance technology, Tham et al. (2016) confirmed that the synergistic adsorption of particles and surfactants can significantly improve the interfacial viscoelasticity. However, the existing research is still controversial about the microscopic stability mechanism under high salinity (>100 g/L); specifically, how salt ions affect the adsorption kinetics of particle interface, and whether there is a concentration window for the synergistic effect between particles and surfactants. These problems restrict the industrial application of foam flooding in deep reservoirs (Li et al., 2024a).

In response to the above challenges, in this work, the performance of five surfactants was systematically evaluated

Table 1. Solution preparation information.

Surfactant solution (mL)	0.1	0.3	0.5	0.7	1
Deionized water (mL)	99.9	99.7	99.5	99.3	99
Concentration (%)	0.1	0.3	0.5	0.7	1

by the Waring-blender method based on the typical deep reservoir conditions of an oilfield in Western China (temperature of 170 °C and salinity of 50-200 g/L). This study breaks through the limitations of traditional static evaluation and focuses on the compression effect of salt ions on the interface electric double layer, as well as the adsorption behavior of core-shell particles at the gas-liquid interface and the comprehensive stability of foam under multi-factor coupling. Through the calculation of foam comprehensive index and the analysis of interfacial interaction, the synergistic stability mechanism of salt-particle-surfactant is revealed, providing a theoretical basis and technical support for the formulation design of foam flooding in deep reservoirs.

2. Experimental methodology

2.1 Materials and apparatus

The experimental materials used in this study included a variety of surfactants and chemical agents sourced from reputable suppliers. Specifically, the surfactants T-A, T-B, and YF-1 were provided by an oilfield in China, while SDS with a purity of 97% and NaCl with a purity of 99.5% were obtained from Shanghai McLean Company. Additional agents such as ZK-1, ZK-2, and ZK-3 were supplied by Qingtian Zhongke Plant Technology Co., Ltd., and a core-shell particle mother liquor was sourced from Jiangsu University, with a molecular weight of 8 kDa and 7% concentration. Deionized water was used throughout the experiments, which was prepared using a Youpu ultrapure water preparation instrument (model UPT-I-10T) with a resistivity of up to 18.25 MΩ·cm, provided by Sichuan Youpu Ultrapure Technology Co., Ltd. Standard laboratory equipment, including a Waring-blender stirrer, measuring cylinders and electronic scales, was used to prepare and handle all experimental solutions.

2.2 Basic performance evaluation

The purpose of the experiment was to explore the foaming performance and optimal concentration of different types of surfactants for subsequent in-depth exploration. The specific solution preparation information is shown in Table 1.

The 100 mL mixed solution was poured into a Waring-blender stirrer, and the rotational speed was set to 8,000 rpm for a stirring duration of 3 min. The generated foam was poured into a 1,000 mL measuring cylinder to read the total volume of the foam, that is, the foaming volume. The time required for the foam to precipitate 50 mL of liquid, that is, the half-life of the liquid, was recorded. At the end of each experiment, deionized water was used to rinse the measuring cylinder and the Waring-blender agitator to ensure that there was no remaining foam in the agitator and the measuring

cylinder. Each experiment was triplicated, the average index was calculated to reduce the influence of error, and the next group of experimental schemes was continued.

2.3 Salinity resistance

The purpose of this experiment was to explore the influence of salinity in formation water on the foam properties of different surfactants (foam volume, half-life of liquid serum), clarify the foaming properties of different surfactants under different salinity environments, and select more suitable surfactants for subsequent experiments. The salinity range of formation water was determined. Since the salinity in typical deep oil and gas reservoirs is mostly 50-200 g/L, the salinity schemes in the experiment were set at 50-200 g/L. The inorganic salts were selected that configure the simulated formation water as NaCl, and the NaCl solids corresponding to the 100 mL solution were calculated to be 5-20 g. The formation water of different salinities were combined with the optimal concentration of the preferred surfactant type, the foaming volume and half-life were respectively recorded, and the salinity resistance properties of the remaining surfactant were further analyzed. Taking 0.5% T-A surfactant + salinity of 50 g/L as an example, the specific steps were as follows: measure out accurately 0.5 mL of T-A surfactant solution and 5 g of NaCl solid, place it in a 100 mL measuring cylinder, then add deionized water to 100 mL, stir and dissolve thoroughly, pour it into a foam stirrer, select 8,000 rpm, and count for 3 min. The subsequent steps were the same as those of the basic performance evaluation experimental steps.

2.4 Aging resistance

Three surfactants-T-A, YF-1, and ZK-1-were selected to establish the experimental system. Under a constant salinity of 200 g/L, thermal aging experiments were conducted using a magnetically stirred high-temperature and high-pressure reactor. The apparatus is equipped with integrated temperature and pressure sensors for the real-time monitoring of experimental conditions and ensure uniform heating of the solution by continuous magnetic stirring. Based on the simulated reservoir conditions, the thermal aging temperature was set to 170 °C, and an 8-day aging study was carried out. By measuring the comprehensive foam index at different aging intervals (0-8 days), the evolution of foam stability in surfactant solutions under high-temperature aging was systematically examined, with a particular focus on elucidating the effect of aging duration on foaming performance and the underlying mechanisms.

2.5 Synergistic action of core-shell particles

The purpose of this experiment was to explore the effect of core-shell particle mother liquor on the foaming properties of T-A surfactants and YF-1 surfactants. Therefore, the design scheme was as follows: 0.5% YF-1, 0.5% YF-1 + 0.2% mother liquor, 0.5% YF-1 + 0.5% mother liquor, 0.5% YF-1 + 0.7% mother liquor, 0.5% YF-1 + 1% mother liquor. There were ten groups of experiments, including 0.5% T-A, 0.5% T-A + 0.2% mother liquor, 0.5% T-A + 0.5% mother liquor, 0.5% T-A + 0.7% mother liquor, and 0.5% T-A + 1% mother liquor. The

Table 2. Combination scheme of salinities and core-shell particle solution concentrations.

Salinity (g/L)	Concentration (%)
0	0
50	0.2
100	0.5
150	0.7
200	1

foaming volume and half-life were respectively recorded. The subsequent steps were the same as the basic performance evaluation experimental steps.

2.6 Synergistic stability

In the experimental scheme, 0.5% T-A surfactant and 0.5% YF-1 were combined with different salinities and different core-shell particle concentrations, and the synergistic effect of the three was analyzed. As shown in Table 1, the salinity was selected as 0 g/L, 50 g/L, 100 g/L, 150 g/L, 200 g/L, and the core-shell particle concentration was selected as 0, 0.2%, 0.5%, 0.7%, 1%. A total of 25 groups of experiments were conducted to analyze the foaming volume and the half-life of the liquid and the comprehensive index of the foam, and to further screen the optimal surfactant scheme. The actual operation steps were the same as above.

3. Experimental results and analysis

3.1 Foam performance evaluation

In order to quantify the difference in the dynamic performance of different types of surfactants, this study used a dynamic stirring method (speed 8,000 rpm, stirring time 3 min) to systematically test the foaming volume, drainage half-life and foam comprehensive index (foaming volume × half-life) of seven surfactants such as T-A and YF-1. A concentration gradient of 0.1%-1% was set in the experiment. The relationship curve between foaming performance and surfactant concentration is shown in Fig. 1.

The change curve of foaming volume with the surfactant concentration could be obtained (Fig. 1(a)). The figure shows that with increasing surfactant concentration, the foaming volume shows a trend of increasing first and then gradually stabilizing. There is a concentration inflection point index, and when the surfactant concentration is less than this index, the corresponding foaming volume change rate is faster, and when it is greater than this index, the corresponding foaming volume change is small or tends to be stable (Joshi et al., 2025). For the inflection point index of the concentration of the seven surfactants, the corresponding index of T-A is 0.5%, the corresponding index of T-B is 0.5%, the corresponding index of YF-1 is 0.5%, the corresponding index of ZK-1 is 0.3%, the corresponding index of ZK-2 is 0.5%, the corresponding index of ZK-3 is 0.3%, and the corresponding index of SDS is 0.5%. Among the seven surfactants, T-A achieved the highest

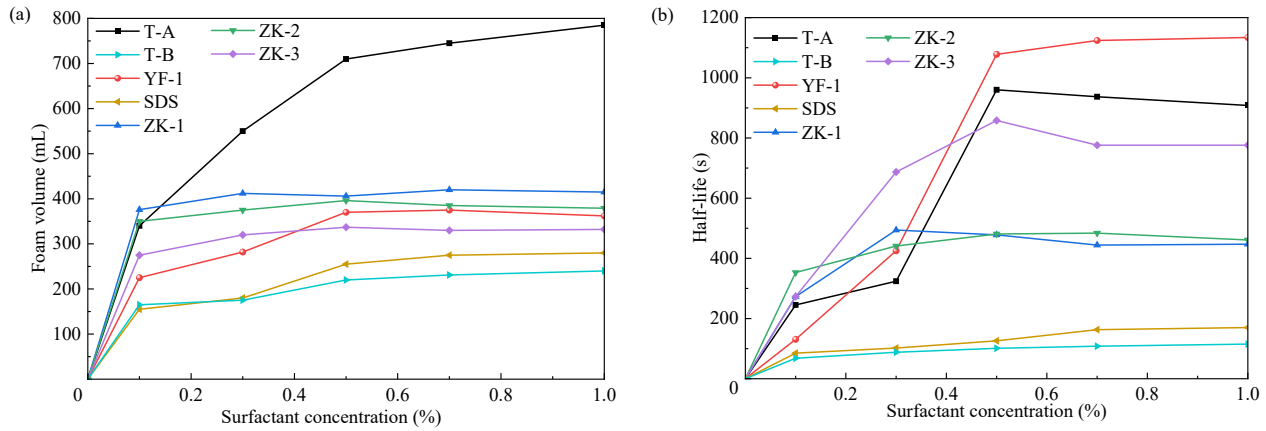


Fig. 1. Relationship between foaming performance and surfactant concentration: (a) Foam volume and (b) half-life.

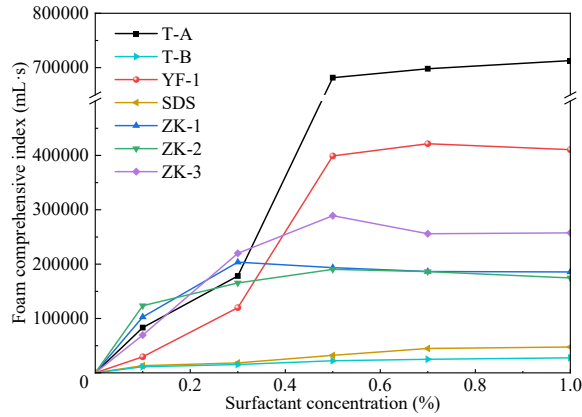


Fig. 2. Relationship between foam comprehensive index and surfactant concentration.

foaming volume of 785 mL. This was 240 mL for T-B, 375 mL for YF-1, 420 mL for ZK-1, 396 mL for ZK-2, 337 mL for ZK-3, and 280 mL for SDS. After the seven surfactants exceeded their respective inflection point concentrations, the comparison of average foaming volume was T-A > ZK-1 > ZK-2 > YF-1 > ZK-3 > SDS > T-B.

Further analysis of Fig. 1(b) shows that the surfactant YF-1 with a general initial foaming volume performed well in foam drainage stability, and ZK-3 with a poor initial foaming volume also had a great improvement in foam stability, while the foams generated by ZK-1 and ZK-2 with higher initial foaming volume also had a shorter drainage half-life. Therefore, considering the two factors of foaming volume and drainage half-life, the product of the two was used as the comprehensive index of the foam, and the comparison under different concentration conditions was made.

From Fig. 2, the concentration inflection points corresponding to the foam comprehensive index curves of different surfactants change slightly, but this also shows that with increasing surfactant concentration, the foam comprehensive index gradually rises and tends to be stable. This is because with increasing concentration, more surfactant molecules are adsorbed at the interface of the foam liquid film, hence the

surface activity gradually increases, and there is a critical micelle concentration, which makes the surfactant molecules at the interface reach the maximum adsorption capacity. With the further increase in concentration, the foam performance changes more smoothly or even slightly lowers (Chen et al., 2024). After the seven surfactants exceed their respective inflection point concentrations, in terms of the comparison of the comprehensive index of the generated foams, T-A > YF-1 > ZK-3 > ZK-1 > ZK-2 > SDS > T-B surfactants. Because the average foam comprehensive index of SDS and B surfactants is much smaller than that of other surfactants, combined with the economic applicability of surfactants, five surfactants T-A, YF-1, ZK-1, ZK-2 and ZK-3 were selected for subsequent evaluation experiments. The corresponding optimal concentrations of T-A, YF-1, ZK-1, ZK-2 and ZK-3 were 0.5%, 0.5%, 0.3%, 0.5% and 0.5%, respectively. Considering the high salinity environment of the actual reservoir, it was still necessary to evaluate the foaming performance of the optimal concentration foam system under different salinity conditions.

3.2 Salinity resistance

The addition of inorganic salts affects the properties of the surfactant solution. Indeed, after performing this step, the ZK-2 surfactant solution showed flocculation, and almost no foam was produced after high-speed stirring. Therefore, the foaming performance curve of ZK-2 was not shown in the salinity evaluation diagram. Although the ZK-3 surfactant solution at high salinity has no flocculation phenomenon, the foam generated after high-speed stirring is abnormally dense. ZK-2 and ZK-3 do not show good compatibility with the simulated formation water.

It can be observed that with the increase in salinity, the foaming volume curves and drainage half-life curves of surfactants T-A, YF-1 and ZK-1 fluctuate slightly and tend to be stable as a whole (Fig. 3). The foaming volume and drainage half-life curve of ZK-3 show a trend of continuous growth. The generated foam has a low volume and an exceptionally prolonged half-life compared to other surfactants, indicating that the generated foam fluidity is poor. The corresponding

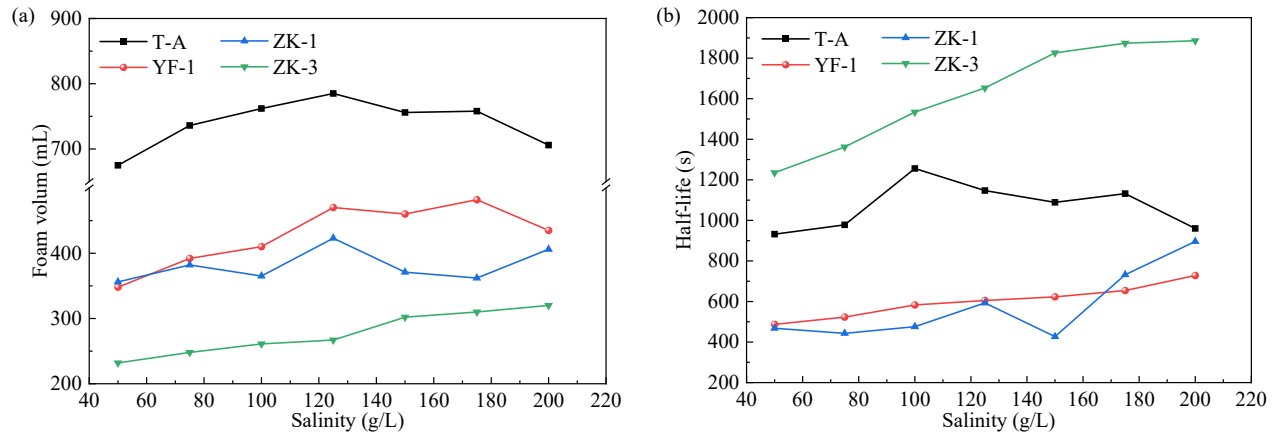


Fig. 3. Relationship between foaming performance and salinity: (a) Foam volume and (b) half-life.

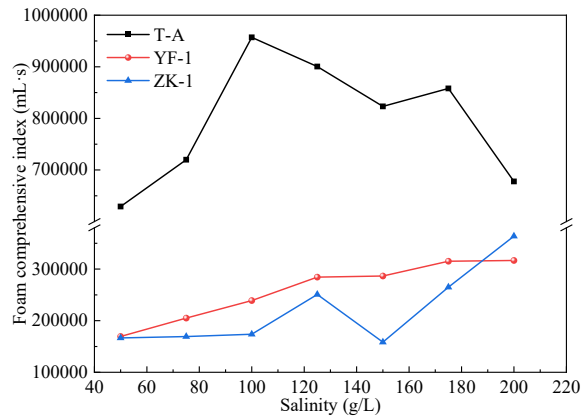


Fig. 4. Relationship between foam comprehensive index and salinity.

foaming volume under the same salinity conditions was ranked as T-A > YF-1 > ZK-1. It can be seen that under the same salinity conditions, the half-life of YF-1 and ZK-1 is close to the T-A, showing a trend of increasing first and then decreasing.

It is shown in Fig. 4 that although the foam comprehensive index curve of T-A surfactant is higher than that of pure water under high salinity conditions, the trend fluctuation is unstable. With the increase in salinity, the foam comprehensive index of T-A surfactant increases first and then decreases. The foam comprehensive index curve of surfactant YF-1 is lower than that of pure water, but the average level of foam comprehensive index is still higher than that of ZK-1. With increasing salinity, the foam comprehensive index of surfactant YF-1 increases steadily, showing good salinity resistance. Furthermore, the foam comprehensive index curve of surfactant ZK-1 shows a fluctuating upward trend, but the foam comprehensive index under some salinity conditions is lower than that under pure water conditions, so the salinity resistance of ZK-1 is not as good as that of YF-1. Although the foam comprehensive index of T-A is much larger than that of YF-1, it is not as good as that of YF-1 in the salinity resistance test. Therefore, after the screening of salinity resistance evaluation experiments,

follow-up experimental evaluation was carried out for YF-1 and T-A. In Fig. 4, it is known that with increasing salinity, the foam comprehensive index of T-A surfactants shows a trend of increasing first and then decreasing. The mechanism is analyzed as shown in Fig. 5.

The addition of inorganic salts to surfactant systems generally enhances their surface-active properties, manifested by marked reductions in both solution surface tension and critical micelle concentration. Experimental studies have demonstrated that appropriate salt addition effectively improves the capacity of surfactants to reduce solvent surface tension (Lin et al., 2025). Surfactant molecules are ionized out of anions and cations in water. These anionic surfactant molecules adsorb at the gas-liquid interface to form a monolayer (Fig. 5(a)), in which the hydrophobic long chain faces the air and the hydrophilic group faces the water phase with a negative charge (Lin et al., 2025). As shown in Fig. 5(b), due to the negative charge of the polar group of the surfactant molecule, it attracts oppositely charged ions (such as Na^+) around it to form an electric double layer (dense layer and dispersion layer). When an appropriate amount of salt solution is added, NaCl dissociates Na^+ and Cl^- , in which Na^+ neutralizes the negative charge of the surfactant molecules, resulting in a decrease in the electrostatic attraction of the negatively charged surfactant molecules in the solution to the Na^+ of the dispersion layer. This eventually leads to the compression of the electric double layer and the closer arrangement of the interface molecules, which more effectively reduces the free energy of the gas-liquid interface and makes this interface more stable. As shown in Fig. 5(c), the electric double layer is compressed and the gas-liquid interface is more stable. As shown in Fig. 5(d), when excessive salt solution is added, excessive electrolyte in the solution may lead to aggregation or precipitation of surfactant molecules, which reduces foam stability (Zhang et al., 2024; Zhou et al., 2025). Therefore, adding an appropriate amount of salt can promote the formation of foam, while the high salinity may destroy the stability of this foam. As shown in Fig. 4, the foam comprehensive index of T-A foaming agent shows a trend of first increasing and then decreasing with increasing salinity. The aggregation

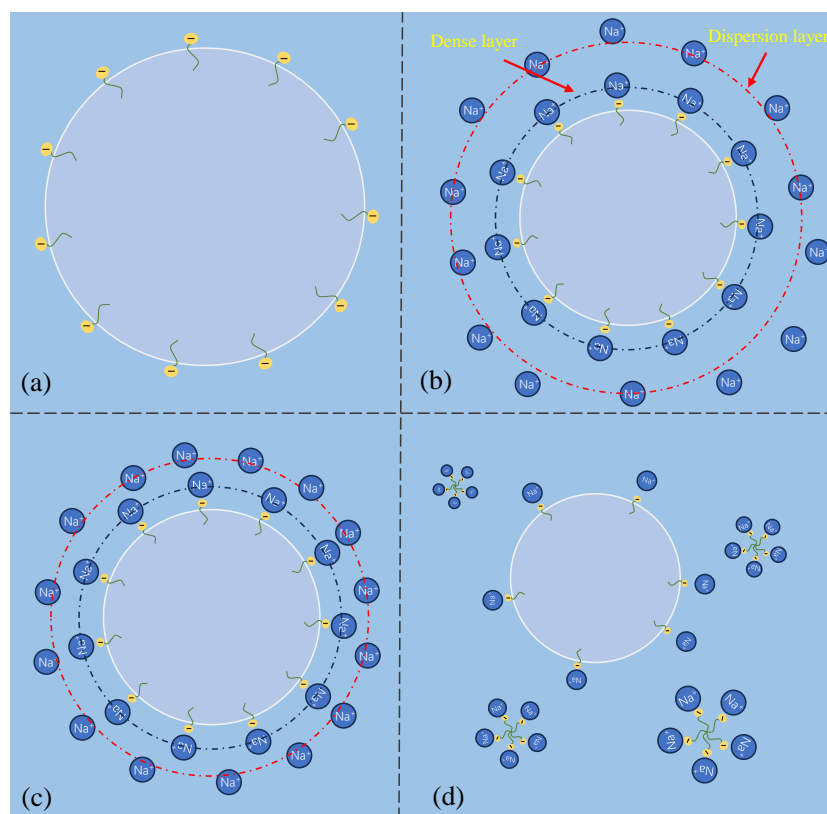


Fig. 5. Distribution of salt ions in the bubble outer layer: (a) Surfactant monolayer, (b) electric double layer, (c) compression electric double layer, and (d) aggregation or precipitation of surfactant molecules.

behavior of surfactant at the oil/water interface also conforms to this law: inorganic salt reduces the electrostatic repulsion of surfactant electrode through the charge shielding effect, while inducing the spatial compression of electric double layer structure when the concentration reaches the optimal value can even reduce the oil/water interface tension to an ultra-low level (Tao et al., 2024). The excellent salinity resistance and chemical stability of T-A under high salinity conditions can be attributed to the fact that its sulfonic acid group overcomes the compression effect of high ionic strength on Debye length through enhanced electric double layer repulsion. This verifies the applicability of the electrostatic stability mechanism in DLVO theory under high salinity conditions.

With increasing salinity, the foam comprehensive index shows a downward trend. In addition to the aggregation or precipitation of surfactant molecules when the added salt is excessive (Fig. 6), the Na^+ dissociated from NaCl is adsorbed around the head group of surfactant molecules, neutralizing some negative charges and reducing the electrostatic repulsion between surfactant molecules, resulting in closer molecular arrangement (Fig. 6(a)). This enhances the stability of the liquid film and slows down the drainage rate of the foam to a certain extent. However, the weakening of electrostatic repulsion also leads to a reduction in the spacing between adjacent bubbles (Fig. 6(b)). This in turn makes it easier for bubbles to coalesce and fuse and ultimately leads to a decrease in the foam comprehensive index, which also explains the reason for the fluctuation of foam comprehensive index of

part surfactants (Anu et al., 2024).

3.3 Aging resistance

As illustrated in Fig. 7, the comprehensive foam index of T-A and YF-1 exhibit minimal fluctuations (less than 5%) during the 2-8 day aging period, indicating their excellent thermal stability. In contrast, ZK-1 demonstrates a pronounced downward trend with aging time, with its foam index ultimately declining by 72%. Comparative analysis reveals that T-A possesses the highest foam performance and superior thermal aging resistance. Conversely, ZK-1 displays significant performance degradation at 170 °C due to its high thermal sensitivity, rendering it unsuitable for application in high-temperature reservoirs.

To identify the most suitable surfactant system for high-temperature and high-salinity reservoirs, a two-factor evaluation experiment assessing both salt tolerance and thermal stability was conducted. This evaluation was supported by key performance indicators such as foam volume and half-life. On the basis of the results, T-A was identified as the optimal surfactant.

From a structure-activity relationship perspective, the molecular design of YF-1 involves a sulfonate-based anionic surfactant as the primary component, chosen for its excellent thermal stability and cost-effectiveness, thereby meeting the thermal requirements of reservoir conditions. An alcohol ether-based nonionic surfactant was introduced to enhance salt tole-

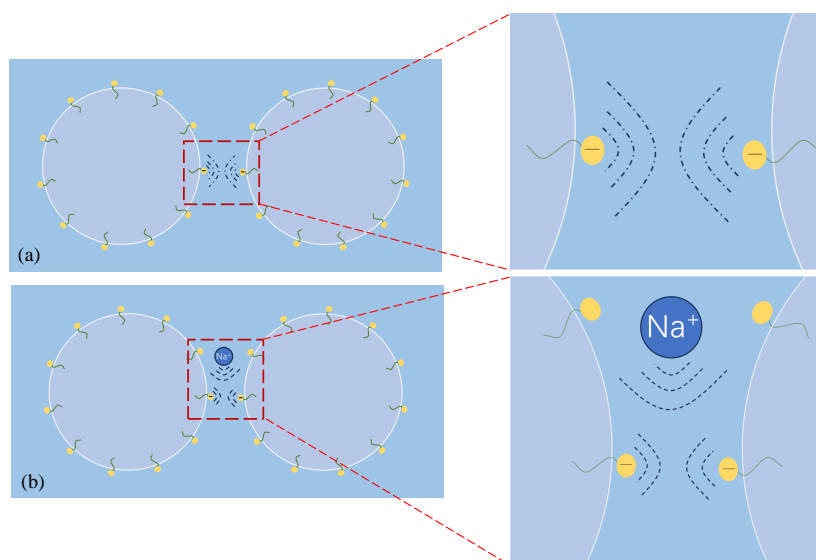


Fig. 6. Schematic of salt ions improving electrostatic repulsion between adjacent bubbles: (a) Electrostatic repulsion and (b) reduction of electrostatic repulsion.

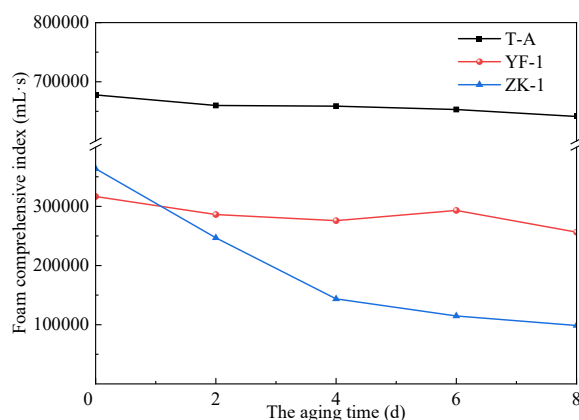


Fig. 7. Relationship between foam comprehensive index and aging time.

rance, and its susceptibility to high-temperature degradation was mitigated through molecular structure optimization. An anionic-nonionic composite system was thus constructed, leveraging the synergistic effects between sulfonate and alcohol ether groups to achieve enhancement in both thermal and salt resistance performance.

3.4 Synergy of core-shell particles

It can be observed that the foam generated by the YF-1 surfactant solution has large bubbles and uneven distribution, while the foam generated by the T-A surfactant solution has no obvious large bubbles, and the bubble size is highly uniform and dense (Fig. 8). The visual observation of the foaming effect of T-A surfactant produces better results. However, after adding different concentrations of mother liquor, the effect of the two was not significantly improved. The foaming volume and drainage half-life of different schemes were recorded as shown in Table 3.

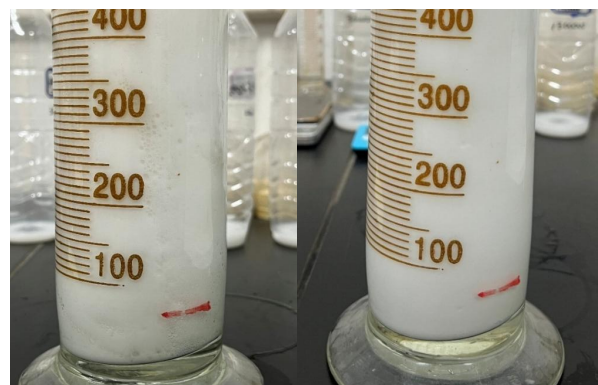


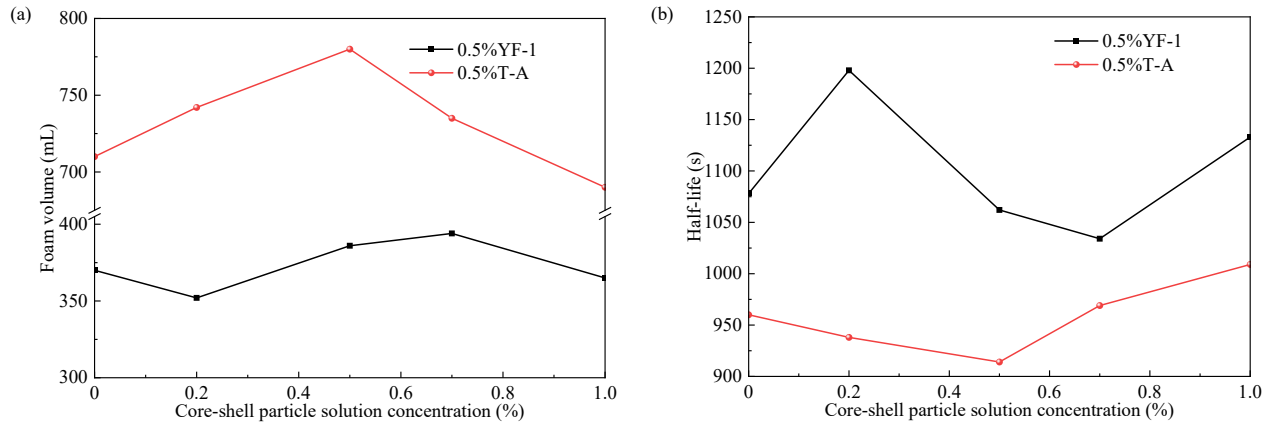
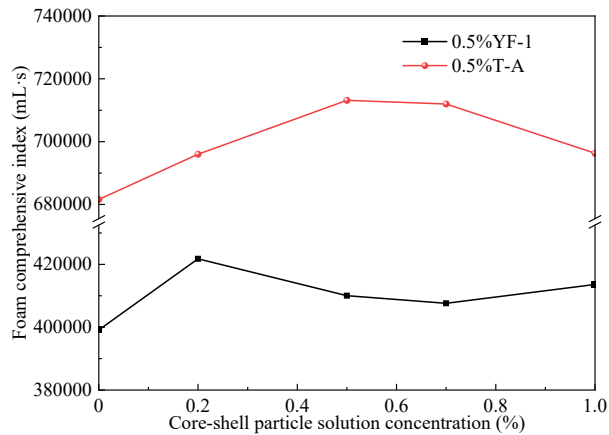
Fig. 8. Left: YF-1 foaming effect. Right: T-A foaming effect.

As shown in Fig. 9, the foaming volume of YF-1 fluctuates greatly at different mother liquor concentrations, and there is no obvious monotonic change trend. Among them, when the mother liquor concentration is 0.7%, the foaming volume reaches the maximum index (394 mL), and then decreases slightly at 1% (365 mL). The foaming volume of T-A increases first and then decreases with the increase in mother liquor concentration, reaching the maximum index (780 mL) at 0.5% mother liquor, and then gradually decreases (690 mL at 1%). Comparing the changes in the foaming volume of the two surfactants with the concentration of the core-shell particles, the foaming volume of the T-A is significantly higher than that of YF-1, indicating its better foaming ability. The addition of core-shell particles has a more obvious effect on the foaming ability of T-A.

The half-life of YF-1 is the highest (1,198 s) when the concentration of mother liquor is 0.2%, indicating that the core-shell particles of this concentration are helpful to improve the foam stability. As the mother liquor concentration increases from 0.2% to 0.7%, the half-life decreases because the excessive accumulation of core-shell particles leads to an increase in the thickness of the foam film, while the strength

Table 3. Foam correlation index of different core-shell particle concentrations.

Combination type	Foaming volume (mL)	Drainage half-life (s)	Foam comprehensive index (mL·s)
0.5% YF-1	370	1,078	399,140
0.5% YF-1+ 0.2% particle	352	1,198	421,780
0.5% YF-1 + 0.5% particle	386	1,062	410,040
0.5% YF-1 + 0.7% particle	394	1,034	407,600
0.5% YF-1 + 1% particle	365	1,133	413,600
0.5% T-A	710	960	681,600
0.5% T-A + 0.2% particle	742	938	696,000
0.5% T-A + 0.5%particle	780	914	713,160
0.5% T-A + 0.7% particle	735	969	712,000
0.5% T-A + 1% particle	690	1,009	696,300

**Fig. 9.** Relationship between foam performance with the concentration of core-shell particles: (a) Foam volume and (b) half-life.**Fig. 10.** Relationship between foam comprehensive index and the concentration of core-shell particles.

of the film decreases (Xu et al., 2024). The half-life rebounds to 1,133 s at 1.0%, because the high concentration of particles forms a denser membrane structure, delaying liquid discharge. The half-life of T-A is slightly lower than that of YF-1, and

it decreases first and then increases with increasing mother liquor concentration, indicating that the stability of core-shell particles on foam T-A is relatively weak, albeit it still has an impact. Comparing the two surfactants, it can be seen that the foam stability of YF-1 is better than that of T-A, especially at 0.2% and 1.0% mother liquor concentration. The half-life of T-A is relatively short, indicating that the foam structure is easy to break and the liquid discharge rate is fast. The results of the synergistic stability experiment of core-shell particles are illustrated in Fig. 10.

The foam comprehensive index of YF-1 reaches the maximum at 0.2% mother liquor, indicating that the core-shell particles of this concentration can significantly improve the foam performance (Fig. 10). As the concentration of the mother liquor increases to 0.7%, the comprehensive index of the foam decreases slightly, but it rises again at 1.0%, indicating that the high concentration of particles still has a certain stabilizing effect. For T-A, the maximum index is reached at 0.5% mother liquor concentration, and then decreases slowly. This indicates that core-shell particles can enhance the comprehensive performance of T-A at appropri-

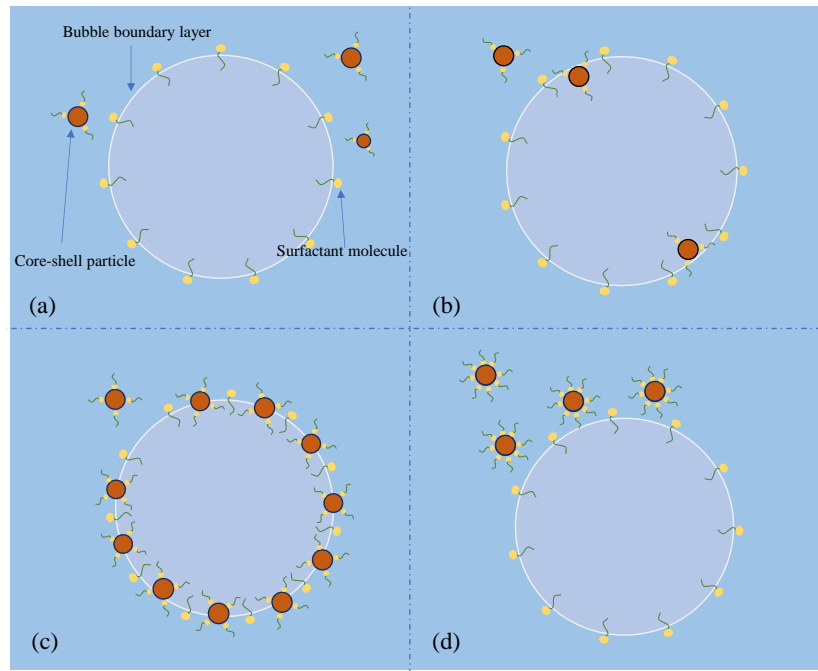


Fig. 11. Foam stabilization mechanism of core-shell particles cooperating with surfactant: (a) Monolayer, (b) core-shell particles added, (c) denser protective layer, and (d) micelles formed.

ate concentrations, while excessive concentrations affect the stability of the foam (Zhang et al., 2025). Comparing the two surfactants, the foam comprehensive index of T-A is much higher than that of YF-1, and the difference between the two foam comprehensive index is the largest at 0.5% mother liquor concentration. The comprehensive index of YF-1 is the best when the mother liquor is 0.2%, but the overall performance is lower than that of T-A. This shows that T-A has better foaming ability and comprehensive performance, while YF-1 is relatively biased towards foam stability.

In the field of nanoparticle-stabilized foam mechanisms, the academic community has established systematic understanding. Wang et al. (2020) experimentally discovered through studies on fly ash particle systems that the oriented adsorption of particles at the liquid film interface produces dual effects: on the one hand, it regulates interfacial tension to reduce the system's energy state; on the other hand, it enhances the elastic modulus in the rheological properties of the liquid film. This synergistic interaction not only effectively suppresses liquid film drainage but also significantly delays the Ostwald ripening and coalescence processes of bubbles. Meanwhile, research by Maestro's team (Maestro et al., 2014) revealed a surfactant-mediated particle assembly mechanism. Their findings demonstrated that under dynamic compression conditions, interface-adsorbed nanoparticles form an energy-dissipating, quasi-solid structure through dense packing. This reversible mechanical response characteristic provides the foam system with a dynamic stabilization mechanism. As shown by the experimental results in Fig. 10, the foam comprehensive parameter exhibits an initial increase followed by a decrease with rising nanoparticle concentration. This trend aligns with interparticle interactions and cooperative foam

stabilization effects, with detailed manifestations illustrated in Fig. 11. As can be seen from Fig. 11(a), the hydrophobic tail end of the surfactant molecule is inserted into the gas phase and the hydrophilic head end is extended into the liquid phase, which is quickly adsorbed on the liquid surface and forms a monolayer, playing a certain role in promoting the stability of the foam and delaying the coalescence of bubbles due to the principle of electrostatic repulsion. As shown in Fig. 11(b), with the core-shell particles added, they are distributed in the bubble boundary layer through hydrophobic interaction, and the surfactant molecules are combined with the core-shell particles to form a macromolecular protection area. This slows down the drainage rate of the bubble boundary and plays a role in stabilizing the foam, as shown in Fig. 11(c). When the concentration of core-shell particles and surfactant solution reaches the optimal value, the core-shell particles synergistically adsorb surfactant molecules to form a denser protective layer at the bubble boundary, achieving the best foam stability. As shown in Fig. 11(d), when the concentration of surfactant solution is too high, micelles are formed, and core-shell particles will not easily form a protective layer at the bubble boundary, making the foam stability decrease (Tran et al., 2023; Ravazzano and Ferreira, 2024).

3.5 Synergistic stability

The foaming volume and half-life data of 0.5% YF-1 and 0.5% T-A of the two surfactants were plotted into a cloud diagram for comparative analysis. The relationship between foaming volume and half-life with salinity and core-shell particle concentration is shown in Fig. 12.

The foaming volume of 0.5% YF-1 fluctuates with the increase in particle concentration when the salinity is 0 g/L,

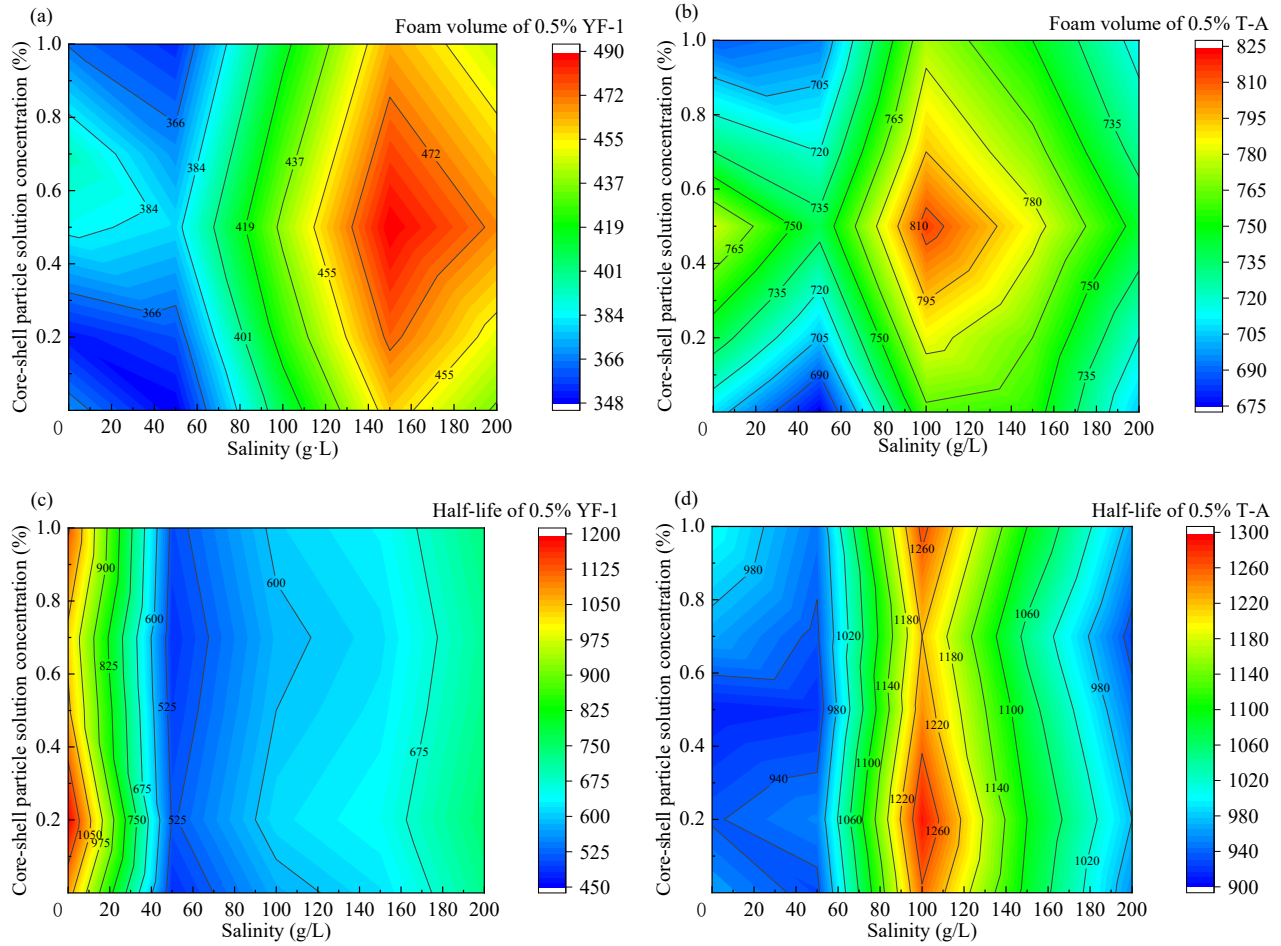


Fig. 12. Relationship between foam performance with salinity and core-shell particle concentration: (a) Foam volume of YF-1, (b) foam volume of T-A, (c) half-life of YF-1, (d) half-life of T-A.

peaks at 0.7%, and falls back to 365 mL at 1.0% (Fig. 12(a)). When the salinity is 100 g/L, with the increase of particle concentration, the foaming volume also increases first and then decreases, but the fluctuation range is small. At high salinity (such as 200 g/L), the volume increases first and then decreases with the increase in particle concentration, and reaches the maximum index at 0.5%. Therefore, the salinity index is fixed, and the vertical observation variation law is observed. The foaming volume of YF-1 generally increases first and then decreases with increasing core-shell particle concentration. By fixing the concentration of core-shell particles and observing the change law horizontally, it can be found that the foaming volume of YF-1 is significantly improved in the low salinity range. At high salinity, YF-1 shows good salt resistance and the volume remains high. For example, at a salinity of 50 to 100 g/L, the volume increases from 380 to 440 mL, while at 200 g/L, there 470 mL is still present. Observing the whole relationship diagram, it can be seen that there is a peak center; when the salinity is 150 g/L and the core-shell particles are 0.5%, the foaming volume can reach the peak.

At a salinity of 0 g/L, the foaming volume of T-A increases first and then decreases with increasing particle concentration, and reaches the maximum at 0.5% (Fig. 12(b)). When the

salinity is 100 g/L, with increasing particle concentration, the foaming volume increases first and then decreases, and reaches the maximum index at 0.5%. When the salinity is 200 g/L, the volume remains high at 0.5% particle concentration. Through the vertical observation of the change law, it is found that the foaming volume of T-A increases first and then decreases with the increasing concentration of core-shell particles, showing an approximate symmetrical distribution relationship. The change rule of transverse observation shows that the foaming volume decreases first, next increases and then decreases with increasing salinity, and reaches the maximum when the salinity is 100 g/L. The overall foaming volume is significantly higher, but when the salinity is higher, the attenuation caused by the salting-out effect is also more obvious. The structural separation pressure induced by the surface roughness of core-shell particles significantly changes the discharge kinetics of the foam liquid membrane. When the concentration of core-shell particles is 0.5%, the pinning effect caused by the lag of contact angle makes the capillary pressure and structural force in the boundary region of the plateau reach a dynamic balance, prolongs the liquid film rupture time, and improves foam stability. This finding provides a theoretical basis for enhancing foam migration stability through interface

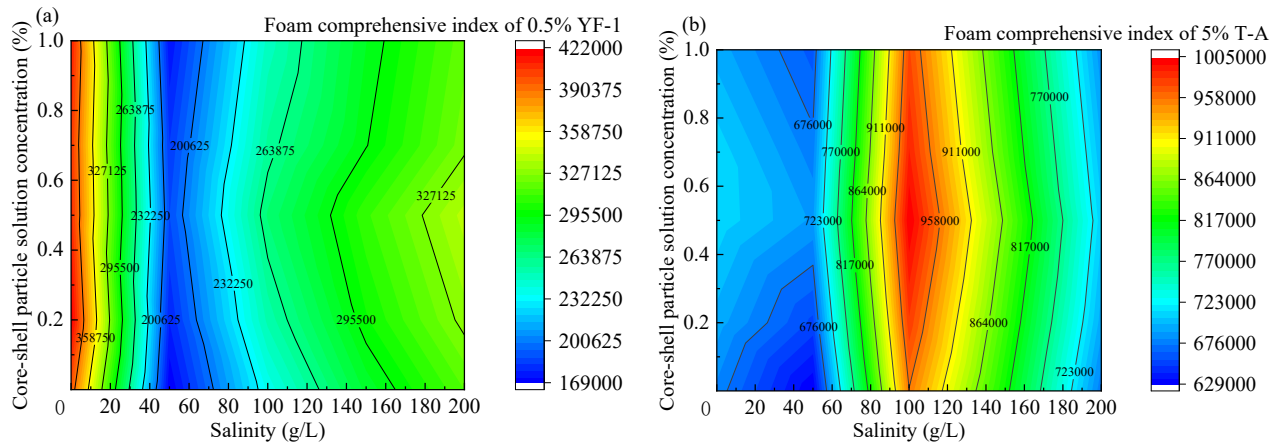


Fig. 13. Relationship between foam comprehensive index, salinity, and the core-shell particle concentration: (a) YF-1 and (b) T-A.

microstructure design in the foam flooding process.

When the salinity is 0 g/L, the half-life of YF-1 reaches the maximum (1,198 s) at 0.2% particle concentration, and decreases due to interfacial rigidity at high concentration (Fig. 12(c)). At a salinity of 200 g/L, the half-life reaches a maximum (730 s) at a particle concentration of 0.5%. By the vertical observation of change law, it can be found that when the salinity is constant, with the increase in the core-shell particle concentration, the half-life shows a trend of increasing first and then decreasing, and the fluctuation range is small. By observing the variation law horizontally, it is found that the half-life decreases first and then increases steadily at a salinity of 0-50 g/L, and there is a trend to reach the initial index. When observing the change relationship of T-A surfactants, it is found that when the salinity is fixed, the half-life decreases first and then increases with increasing particle concentration, the half-life fluctuation range is not large, and the particles only slightly improve the stability (Fig. 12(d)). Under high salt conditions, half-life is significantly shortened, and the salting-out effect weakens the strength of the interfacial film.

The relationship between the comprehensive index of the foam, the salinity, and the concentration of the core-shell particles is shown in Fig. 13. Referring to Fig. 13, the foam comprehensive index of YF-1 is less affected by the concentration of core-shell particles and is greatly affected by salinity. When the salinity is in the range of 0-50 g/L, the foam comprehensive index shows a downward trend. When the salinity is 50-200 g/L, the comprehensive index shows a gradual upward trend and has a tendency to reach the initial index, indicating that YF-1 has better salt resistance under high salinity conditions. From the diagram, it can be seen that the foam comprehensive index of T-A is also relatively less affected by the concentration of core-shell particles but is greatly affected by salinity. With increasing salinity, the comprehensive index shows a trend of increasing first and then decreasing, reaching the maximum at a salinity of 100 g/L, but the degree of fluctuation is more obvious. The salt resistance of T-A surfactants is relatively poor. Therefore, the comprehensive index of YF-1 depends on the stable growth

of particle salt resistance in a high salt environment, making it suitable for harsh conditions. The comprehensive index of T-A surfactants is relatively higher, but it needs to rely on particle buffering when the salt concentration is high, and the attenuation range is greater.

Future research needs to deepen the theory and application of high-salinity foam flooding from multiple dimensions. Firstly, microfluidic chips and high-temperature and high-pressure visualization devices should be combined to observe the interface evolution process of foam under dynamic shear stress in real time, and a multiphase flow numerical model including particle adsorption kinetics and salting-out effect should be established to predict the migration law of foam in porous media (Wang et al., 2025). Secondly, the intelligent composite system of responsive core-shell particles and bio-based surfactants (such as sophorolipids) can be developed, and the interface suitability can be optimized by molecular design to achieve the accurate regulation of foam stability (Liu et al., 2019; Abu Zaid et al., 2025). It is necessary to carry out field pilot tests, use optical fiber monitoring and machine learning algorithms (such as random forest) to track foam dynamics and optimize injection parameters, and explore the influence mechanism of CO₂ phase transition and crude oil composition on foam performance, revealing the synergistic effect of salt-oil-water-particle four-phase system (Li et al., 2025; Lu et al., 2025a, 2025b). Finally, integrating the demand for low-carbon technologies, a CO₂-foam-nanoparticles composite system can be constructed to improve the carbon sequestration efficiency, and the synergistic mode of foam flooding and microbial flooding can be explored to promote the development of ‘physical-chemical-biological’ multi-scale oil displacement technology (Song et al., 2019; Zhang et al., 2021; Seright and Wang, 2023; Wang et al., 2024).

4. Conclusions

(1) Among the seven surfactants, T-A and YF-1 shows good temperature and salinity resistance, and YF-1 has higher foam stability. T-A is characterized by both the highest foam comprehensive index and the optimal aging resistance. At the

optimal mass concentration of 0.5%, the foam comprehensive value of T-A was as high as 681, 600 mL·s.

(2) In a high salinity environment, the core-shell particles interact with the adsorption of surfactant molecules to form a denser protective layer at the bubble boundary, yielding the best the foam stability. The combination of 0.5% concentration of T-A and 0.5% mass fraction of core-shell particles achieves a higher foam comprehensive index.

(3) Morphological analysis reveals that the foam particle size generated by T-A is small and evenly distributed. The excellent salt resistance and chemical stability of T-A under high salinity conditions can be attributed to the fact that its sulfonic acid group overcomes the compression effect of high ionic strength on Debye length through enhanced electric double layer repulsion.

(4) The core-shell particles are closely arranged on the foam liquid membrane, the discharge rate is delayed by the structural separation pressure induced by surface roughness, and the capillary pressure and structural force in the boundary region of the plateau are dynamically balanced by the contact angle lag, so as to improve the foam stability.

Acknowledgements

The authors gratefully acknowledge the financial support of the Open Research Fund of State Key Laboratory of Deep Oil and Gas (No. SKLDOG2024-KFYB-14), Natural Science Research Project of Jiangsu Higher Education Institutions (No. 23KJB440001).

Conflict of interest

The authors declare no competing interest.

Open Access This article is distributed under the terms and conditions of the Creative Commons Attribution (CC BY-NC-ND) license, which permits unrestricted use, distribution, and reproduction in any medium, provided the original work is properly cited.

References

- Abu Zaid, N. S. K., Johar, A., Nasser, M. S., et al. Synergistic effect of chemical and bio-based surfactants in stabilizing nanoemulsions. *Geoenergy Science and Engineering*, 2025, 247: 213663.
- Akamine, T., Tosuai, T., Ramadhan, R., et al. Visualizing oil displacement by nanofluids at pore scale: A concentration-dependent nanofluid spreading induced by structural disjoining pressure. *Capillarity*, 2024, 12(1): 17-26.
- Anu, M. A., Tomy, M., Gopi Krishnan, R., et al. Enhanced electrochemical properties of cobalt oxide nanoparticle electrode modified with low concentration of cationic surfactant. *Journal of Electroanalytical Chemistry*, 2024, 961: 118225.
- Bello, A., Dorhjie, D. B., Ivanova, A., et al. A numerical feasibility study of CO₂ foam for carbon utilization and storage in a depleted, high salinity, carbonate oil reservoir. *Scientific Reports*, 2024, 14(1): 20585.
- Bersenev, E. A., Matthews, L., Rein, V., et al. Balance of hydrophobic and electrostatic interaction of polymers and surfactants: Case of anionic surfactant and hydrophobically modified polymer. *Journal of Colloid and Interface Science*, 2025, 693: 137572.
- Chen, J., Hou, L., Nan, J., et al. Prediction of critical micelle concentration (CMC) of surfactants based on structural differentiation using machine learning. *Colloids and Surfaces A: Physicochemical and Engineering Aspects*, 2024, 703: 135276.
- Dehdari, B., Parsaei, R., Riazi, M., et al. Dimensionless analysis of foam stability for application in enhanced oil recovery. *Scientific Reports*, 2024, 14(1): 29842.
- Fujii, S. Foams/bubbles stabilized with polymer particles. *Current Opinion in Colloid & Interface Science*, 2024, 72: 101808.
- Gbadamosi, A., Badmus, S. O., Haruna, K., et al. Surfactant applications in oil and gas industry: Efficiency, toxicity, and remediation techniques. *Journal of Molecular Liquids*, 2025, 427: 127440.
- Joshi, D., Ramesh, D. N., Prakash, S., et al. Formulation and characterisation of polymer and nanoparticle-stabilized anionic surfactant foam for application in enhanced oil recovery. *Surfaces and Interfaces*, 2025, 56: 105615.
- Li, K., Li, Y., Wang, W. Intelligent light-driven polystyrene foams for water purification and research into their functionality: Superhydrophobic, self-cleaning, oil-water separation, and photothermal conversion. *Journal of Hazardous Materials*, 2025, 489: 137611.
- Li, Q., Wang, Y., Wei, B., et al. Imbibition oil recovery from tight reservoir cores using microemulsion: Experiment and simulation. *Capillarity*, 2024a, 10(2): 38-47.
- Li, Y., Yang, Y., Dong, M. CO₂ capillary trapping in layered sandstone dominated by inertial force and gravity. *Capillarity*, 2024b, 10(1): 22-28.
- Lin, H., Zhou, Y., Jiang, B., et al. Effect on solution temperature on diffusion for water molecules and molecular characterization of lignite adsorbed ionic surfactants. *Construction and Building Materials*, 2025, 471: 140695.
- Liu, Z., Ghatkesar, M. K., Sudhölter, E. J. R., et al. Understanding the cation-dependent surfactant adsorption on clay minerals in oil recovery. *Energy & Fuels*, 2019, 33(12): 12319-12329.
- Lu, J., He, X., Li, B., et al. Super-wetting cu-mof-based foam for efficient oil/water separation and photothermal cleanup of crude oil. *Separation and Purification Technology*, 2025a, 353: 128483.
- Lu, Y., Zhao, Y., Chen, Z., et al. Bioinspired superhydrophobic polysulfone foams with micro/nano hierarchical structures for highly efficient solar-assisted cleanup of viscous crude oil. *Applied Surface Science*, 2025b, 682: 161702.
- Maestro, A., Rio, E., Drenckhan, W., et al. Foams stabilised by mixtures of nanoparticles and oppositely charged surfactants: Relationship between bubble shrinkage and foam coarsening. *Soft Matter*, 2014, 10(36): 6975-6983.
- Ravazzano, C., Ferreira, G. A. The influence of bilayer fluidity on the stability of aqueous foams made from surfactant vesicle dispersions. *Journal of Molecular Liquids*, 2024, 397: 124136.
- Seright, R. S., Wang, D. Polymer flooding: Current status and

- future directions. *Petroleum Science*, 2023, 20(2): 910-921.
- Shao, W., Yang, J., Wang, H., et al. Recent research progress on imbibition system of nanoparticle-surfactant dispersions. *Capillarity*, 2023, 8(2): 34-44.
- Song, Z., Chen, S., Zhao, F., et al. Whole metagenome of injected and produced fluids reveal the heterogenetic characteristics of the microbial community in a water-flooded oil reservoir. *Journal of Petroleum Science and Engineering*, 2019, 176: 1198-1207.
- Sun, J., Dai, L., Lv, K., et al. Recent advances in nanomaterial-stabilized pickering foam: Mechanism, classification, properties, and applications. *Advances in Colloid and Interface Science*, 2024a, 328: 103177.
- Sun, Y., Jia, Z., Yu, B., et al. Research progress of nanoparticles enhanced carbon dioxide foam stability and assisted carbon dioxide storage: A review. *Chemical Engineering Journal*, 2024b, 495: 153177.
- Tao, W., Jiang, B., Zheng, Y., et al. Molecular dynamics study on the effect of inorganic salts on the wettability of surfactants on bituminous coal: Sodium dodecyl sulfate and sodium chloride as representatives. *Fuel*, 2024, 359: 130397.
- Tham, Y. Y., Molino, P. J., Higgins, M. J., et al. The study of deposition of wood extractives and model compound colloids onto chromium and cellulose surfaces using quartz crystal microbalance with dissipation (QCM-D). *Colloids and Surfaces A: Physicochemical and Engineering Aspects*, 2016, 491: 1-11.
- Tran, T., Gonzalez Perdomo, M. E., Haghighi, M., et al. Effects of cationic and anionic surfactants on the stability, rheology and proppant suspension of nanoparticle-stabilized fracturing foams at elevated temperature. *Geoenery Science and Engineering*, 2023, 228: 212041.
- Vavra, E., Puerto, M., Biswal, S. L., et al. A systematic approach to alkaline-surfactant-foam flooding of heavy oil: Microfluidic assessment with a novel phase-behavior viscosity map. *Scientific Reports*, 2020, 10(1): 12930.
- Wang, K., Xu, M., Zhou, B., et al. Study on the effects of inorganic salts and ionic surfactants on the wettability of coal based on the experimental and molecular dynamics investigations. *Energy*, 2024, 300: 131610.
- Wang, T., Fan, H., Yang, W., et al. Stabilization mechanism of fly ash three-phase foam and its sealing capacity on fractured reservoirs. *Fuel*, 2020, 264: 116832.
- Wang, Y., Wu, M., Hao, Y., et al. Surfactant-mediated transport of copper oxide nanoparticles in porous media: Effects of electrolytes, phosphate and organic matter. *Chemical Engineering Research and Design*, 2025, 217: 283-294.
- Xu, H., Yu, Y., Weng, L., et al. Effect of structural design of core-shell particles and core-shell-shell particles on pvdf dielectric energy storage composite films. *Journal of Materials Research and Technology*, 2024, 31: 3320-3331.
- Zhang, J., Niu, Q., Gao, Y., et al. The aggregation structure and rheological properties of catanionic surfactant mixtures and potential applications in fracturing fluids. *Journal of Molecular Liquids*, 2024, 407: 125118.
- Zhang, L., Xie, J., Luo, X., et al. Enhanced hydrophobicity of shell-ligand-exchanged ZIF-8/melamine foam for excellent oil-water separation. *Chemical Engineering Science*, 2023, 273: 118663.
- Zhang, Y., Liu, Q., Ye, H., et al. Nanoparticles as foam stabilizer: Mechanism, control parameters and application in foam flooding for enhanced oil recovery. *Journal of Petroleum Science and Engineering*, 2021, 202: 108561.
- Zhang, Z., Qiao, M., Zhao, H., et al. Investigating the effect of hydrophilic SiO₂ nanoparticles on foam stability using molecular dynamics simulation. *Colloids and Surfaces A: Physicochemical and Engineering Aspects*, 2025, 712: 136429.
- Zhou, L., Liu, Z., Wang, Y. Molecular insights: How counterions determine surfactant aggregation. *Advances in Colloid and Interface Science*, 2025, 341: 103484.
- Zhou, Y., Tian, Y., Zhang, M. Technical development and application of supercritical CO₂ foaming technology in pcl foam production. *Scientific Reports*, 2024, 14(1): 6825.